IEEE Access
Multidisciplinary | Rapid Review | Open Access Journal

Received February 15, 2021, accepted April 7, 2021, date of publication April 14, 2021, date of current version April 28, 2021.

Digital Object Identifier 10.1109/ACCESS.2021.3073247

An Information Theoretical Analysis of Gap Junction Channels

FARROKH HEJRI[1], MLADEN VELETIĆ[2], AND ILANGKO BALASINGHAM[1,2], (Senior Member, IEEE)

[1]Department of Electronic Systems, Norwegian University of Science and Technology, 7491 Trondheim, Norway
[2]The Intervention Centre, Oslo University Hospital, 0027 Oslo, Norway

Corresponding author: Farrokh Hejri (farrokh.hejri@ntnu.no)

This work was supported by the Research Council of Norway through the Wireless In-body Sensor and Actuator Networks (WINNOW) Project under Grant 270957.

ABSTRACT The propagation of molecules, ions and electrochemical signals in various cell types occurs through hundreds of gap junction channels. A gap junction channel is composed of hundreds of units which are further decomposed to hemichannels. From the computational modeling perspective, each gap junction channel acts as a state machine, switching between different permeability states at known rates. Both the permeabilities and the rates jointly depend on transmembrane and transjunctional voltages. To the best of our knowledge, the effects of the permeability states on the communication performance between cells remain unknown to-date. Here, we use the example of gap junctions between cardiac myocytes (cardiomyocytes) to model a gap junction channel as a finite-state channel. We then apply the Shannon's information theory to compute the achievable information rates. Our results demonstrate the information theoretical limits of communication over cardiac gap junction channels. The proposed analysis is anticipated to address open-research problems in cardiac modeling, as well as in nano-networking where man-made miniature devices inter-connect with cardiomyocytes to enable novel groundbreaking applications in healthcare.

INDEX TERMS Biological information theory, biomedical communication.

I. INTRODUCTION

The concept of intra-body communications (IBC) utilizes the human body as a communication medium for propagation of electromagnetic signals, aiming to wirelessly inter-connect implanted nodes which serve for a specific healthcare application. IBC scenarios usually deploy sophisticated transceivers which provide data transmission using advanced encoding and compression [1].

With the conceptual advent of bionanomachines capable of transceiving electrochemical signals [2], researchers have been proposing numerous solutions for realizing nanoscale communications over the last decades. Coordination through communication capabilities enables bionanomachines to perform more complex tasks, ranging from disease detection to nanosurgery and drug delivery [3]. In addition, the Molecular Communication (MC) paradigm provides a novel systems approach for elucidating the principles of molecular and biological phenomena [4]. Although MC promises a variety of groundbreaking application domains where classical communications show limitations, intra-body nanocommunication networks are the major motivation behind this paradigm [4]. Application examples include molecular-level detection of viruses and bacteria, personalised nanomedicine with pharmacokinetic modelling and biodistribution estimation, and pervasive networks of future biological embedded computing devices (Bio-NanoThings) under the novel communication concept called the Internet of Bio-NanoThings (IoBNT) [5], [6]. According to [7], the main challenge in realizing IoBNT networks lies in the communication interfaces between bionanomachines and biological cells. The communication interfaces in such scenarios are studied in several works through channel modeling [8]–[11], including the possibility of using electromagnetic waves for communication between nanomachines [8], deriving channel impulse response for MC systems [9], and proposing transmitter and receiver architectures towards the realization of transceiver (bio)nanomachines [11]. More advanced scenarios about mobile bionanomachines which can communicate while moving are introduced in [12].

An interconnected network of bionanomachines and biological cells potentially leads to disrupting medical applications. In this study, we are interested in a scenario where bionanomachines interconnect with cardiomyocytes,

The associate editor coordinating the review of this manuscript and approving it for publication was György Eigner.

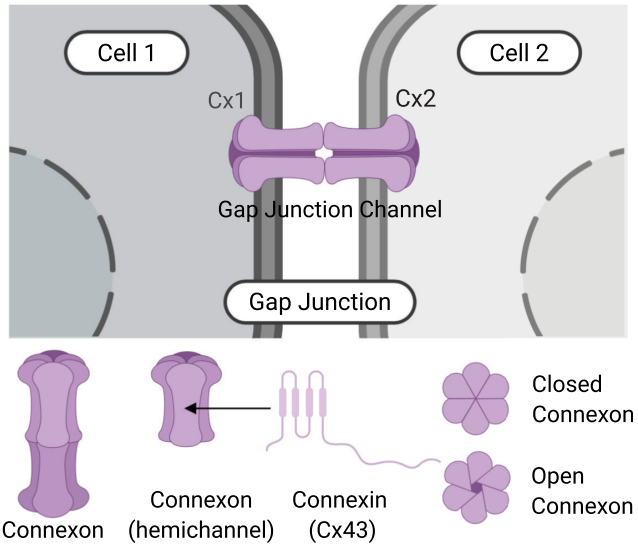

FIGURE 1. An illustration of two connexons forming a gap junction channel.

potentially leading to disrupting applications in cardiac pacing and heart resynchronization therapy. In such a scenario, gap junctions can act as the communication interface. However, for studying the possibility of using gap junctions as communication channels, it is required to explore their communication theoretical characteristics. An important task refers to unveiling their information theoretical limits.

Developing information- and communication theoretical models of IBC, e.g., for carrier frequency optimization, channel characterization and modulation techniques analyses, facilitates future research in this area [13]. Information theory quantifies the achievable amount of information which a communication scheme can convey given any degree of noise contamination. Information theory has been a subject of interest in IBC during the recent years. Examples include [8], which has investigated the capacity of intra-body terahertz nanonetworks, and [14], which has presented an information theoretical analysis on neuro-transmission channels. An extensive study on the information theory of molecular communications between two nodes using biotic/antibiotic objects is done in [15] and [16].

The electrical response of cardiac gap junctions is usually described in terms of conductances as functions of the voltages across the junctions. A single gap junction channel is then further modeled as a serial combination of two hemichannels, each of them assigned to one of the two interconnected cells, whose conductances are modeled as first-order two-state processes [17]–[21]. Fig. 1 illustrates how a single gap junction channel is formed by two hemichannels (connexons), with each connexon further decomposed to six smaller units called connexins. Cardiac gap junctions have non-ohmic and non-linear conductances. The dynamics of their non-linearity have been studied in many works, including [22]–[25]. Gap junctions have also been proposed as media of communication between nanodevices [26]. Subsequently, an information theoretical analysis on gap junction channels has been initially proposed in [27], where the simplifying assumptions of ohmic and constant conductances have been made. Thereby, a novel and more precise information theoretical analysis which considers non-linear dynamics of cardiac gap junctions is necessary.

In this paper, we study the information capacity of gap junction channels. We ground the analysis on our channel model presented in [10]. The model involves four different states for the considered gap junction. First, we calculate the total conductance of the gap junction based on the non-linear dynamic model in each state. Then, we derive the closed-form expressions for noise in each state and utilize them to compute the information capacity using the Gaussian channel model. Ultimately, we derive the total capacity of the gap junction channel using an information theoretical finite-state channel model.

The rest of the paper is structured as follows. Section II introduces the system model. Section III presents the information capacity derivation. Section IV shows the numerical results. Finally, Section V concludes the paper.

II. SYSTEM MODEL

In this section, we first present the basic model from [20] on which the information theoretical analysis presented in the next section is based. Subsequently, we consider the effect of a minor membrane potential gating which we added to the model in our previous work [10]. This phenomenon does not affect the dynamics of the state-machine, but rather introduces a small conductance offset if any of the hemichannels are in their *high* state. This offset, in turn, ensures more accurate expression of noise when computing the capacity.

A. THE TWO-HEMICHANNEL GAP JUNCTION MODEL

The total single branch gap junction model is depicted in Fig. 2. In this subsection, we describe the basic two-hemichannel model from [20] which corresponds to the given block diagram when the g_{m1} and g_{m2} blocks are excluded. We include these blocks in our analysis later in Section II-B to account for the membrane potential effect [10], [28].

In the model, a single gap junction branch is divided into two hemichannels. Each hemichannel is assumed to switch between two main conductance states - *high* and *low* - such that the hemichannel is in the *high* conductance state when the voltage on it is close to zero, and is otherwise in the *low* conductance state.

The model is shown as a serial combination of two hemichannels, Cx1 and Cx2. The transjunctional voltage is denoted as V_j and the membrane potentials of the two neighboring cells 1 and 2 are denoted as V_{m1} and V_{m2}, respectively. According to Kirchhoff's law,

$$V_j = V_{m2} - V_{m1} \tag{1}$$

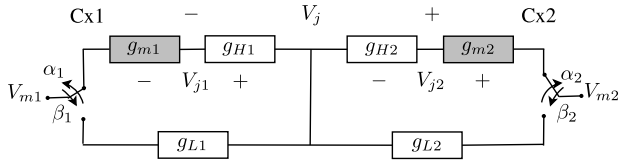

FIGURE 2. Block diagram of a single gap junction branch. V_{j1} and V_{j2} are the voltages on hemichannel 1 and 2, respectively. V_{m1} and V_{m2} are the membrane potentials of cell 1 and cell 2, respectively, which are on the outer sides of the switches.

and

$$V_j = V_{j2} + V_{j1}, \tag{2}$$

where V_{j1} and V_{j2} are the voltages across Cx1 and Cx2, respectively. The conductances in both states are nonlinearly dependent on the voltage across the hemichannel. We assume the relationship between the hemichanel conductances and the voltage drop across the hemichannels to be exponential. This is mainly due to the experimental results showing that this relationship is best approximated by a single exponential function [20]. Mathematically,

$$\begin{aligned} g_{H_1} &= \lambda_{H_1} e^{-\frac{V_{j1}}{V_{0_{H_1}}}}, \\ g_{L_1} &= \lambda_{L_1} e^{-\frac{V_{j1}}{V_{0_{L_2}}}}, \end{aligned} \tag{3}$$

where g_{H_1} is the conductance of the *high* state and g_{L_1} is the conductance of the *low* state for Cx1. The parameters $\lambda_{H_1}, \lambda_{L_1}, V_{0_{H_1}}$ and $V_{0_{L_1}}$ are constants which depend on the type of the hemichannel. According to [20], λ_H is always greater than λ_L for all hemichannel types, but there is no such restriction for V_{0_H} and V_{0_L}. Similarly,

$$\begin{aligned} g_{H_2} &= \lambda_{H_2} e^{-\frac{V_{j2}}{V_{0_{H_2}}}}, \\ g_{L_2} &= \lambda_{L_2} e^{-\frac{V_{j2}}{V_{0_{L_2}}}}, \end{aligned} \tag{4}$$

for Cx2.

For each hemichannel, a 'switch' governed by the hemichannel voltage controls transition between the two states. For Cx1, for example, the rate for a transition from a *high* to a *low* state is represented by α_1. Conversely, a transition from a *low* to a *high* state is represented by β_1. These rates are exponentially related to V_{j_1}. Mathematically,

$$\begin{aligned} \alpha_1 &= \alpha_{01} e^{\frac{V_{j1}}{V_{0_{\alpha_1}}}}, \\ \beta_1 &= \beta_{01} e^{\frac{V_{j1}}{V_{0_{\beta_1}}}}, \end{aligned} \tag{5}$$

where $\alpha_{01}, \beta_{01}, V_{0_{\alpha_1}}$ and $V_{0_{\beta_1}}$ are constants.

Assuming that g_1 and g_2 are the total conductances of Cx1 and Cx2 in Fig. 2, respectively, it follows that

$$\begin{aligned} g_1 &= \lambda_1 e^{\frac{-V_{j1}}{V_1}}, \\ g_2 &= \lambda_2 e^{\frac{-V_{j2}}{V_2}}, \end{aligned} \tag{6}$$

where

$$\begin{aligned} V_{j1} &= V_j \left(\frac{g_2}{g_1 + g_2} \right), \\ V_{j2} &= V_j \left(\frac{g_1}{g_1 + g_2} \right), \end{aligned} \tag{7}$$

and

$$(\lambda_1, V_1) = \begin{cases} (\lambda_{H1}, V_{0_{H_1}}) & \text{for } \textit{high} \text{ state} \\ (\lambda_{L1}, V_{0_{L_1}}) & \text{for } \textit{low} \text{ state}, \end{cases} \tag{8}$$

$$(\lambda_2, V_2) = \begin{cases} (\lambda_{H2}, V_{0_{H_2}}) & \text{for } \textit{high} \text{ state} \\ (\lambda_{L2}, V_{0_{L_2}}) & \text{for } \textit{low} \text{ state}. \end{cases} \tag{9}$$

The numerical values of the abovementioned parameters can be found in Appendix. Since the conductances in Eq. (6) are interrelated, the transition rates are defined between the *joint state* of the two hemichannels in [20] as

$$Q = \begin{array}{c} \\ \text{HH} \\ \text{LH} \\ \text{HL} \\ \text{LL} \end{array} \begin{array}{c} \begin{array}{cccc} \text{HH} & \text{LH} & \text{HL} & \text{LL} \end{array} \\ \begin{bmatrix} -(\beta_1 + \beta_2) & \alpha_1 & \alpha_2 & 0 \\ \beta_1 & -(\alpha_1 + \beta_4) & 0 & \alpha_4 \\ \beta_2 & 0 & -(\alpha_2 + \beta_3) & \alpha_3 \\ 0 & \beta_4 & \beta_3 & -(\alpha_3 + \alpha_4) \end{bmatrix} \end{array},$$

where

$$\begin{aligned} \alpha_1 &= \alpha_{01} e^{\frac{V_{LH1}}{V_{\alpha 1}}}, \\ \alpha_2 &= \alpha_{02} e^{\frac{V_{HL2}}{V_{\alpha 2}}}, \\ \alpha_3 &= \alpha_{01} e^{\frac{V_{LL1}}{V_{\alpha 1}}}, \\ \alpha_4 &= \alpha_{02} e^{\frac{V_{LL2}}{V_{\alpha 2}}}, \\ \beta_1 &= \beta_{01} e^{\frac{V_{HH1}}{V_{\beta 1}}}, \\ \beta_2 &= \beta_{02} e^{\frac{V_{HH2}}{V_{\beta 2}}}, \\ \beta_3 &= \beta_{01} e^{\frac{V_{HL1}}{V_{\beta 1}}}, \\ \beta_4 &= \beta_{02} e^{\frac{V_{LH2}}{V_{\beta 2}}}. \end{aligned} \tag{10}$$

The matrix Q is a transition rate matrix. Therefore, the diagonal elements are defined such that the columns sum to zero. The aforementioned rate coefficients are calculated numerically in Appendix. A representation of the Markov chain corresponding to Q is shown in Fig. 3. According to [20], the state machine is governed by the classical reaction kinetics as

$$\frac{d\vec{n}(t)}{dt} = Q\vec{n}(t), \tag{11}$$

where the state vector $\vec{n}$ is defined as

$$\vec{n} = \begin{bmatrix} n_1 \\ n_2 \\ n_3 \\ n_4 \end{bmatrix},$$

in which the parameters n_1, n_2, n_3, n_4 are the fractions of the channels in the states HH, LH, HL and LL, respectively. Also,

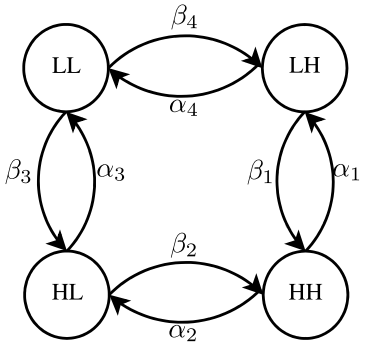

FIGURE 3. Markov chain representation of a four-state gap junction.

the steady-state value of $\vec{n}$ is calculated in [20] as

$$\vec{n}_\infty = A^{-1}\begin{bmatrix}0\\0\\0\\1\end{bmatrix},$$

$$A = \begin{bmatrix}-(\beta_1+\beta_2) & \alpha_1 & \alpha_2 & 0\\ \beta_1 & -(\alpha_1+\beta_4) & 0 & \alpha_4\\ \beta_2 & 0 & -(\alpha_2+\beta_3) & \alpha_3\\ 1 & 1 & 1 & 1\end{bmatrix}.$$

According to [29], the overall conductance of the gap junction can be written as

$$g_t = N_{\text{channel}}[n_1 g_{HH} + n_2 g_{LH} + n_3 g_{HL} + n_4 g_{LL}], \quad (12)$$

where N_{channel} represents the number of channels per gap junction. The conduction scenarios are assumed based on the velocity of the conduction [29]:

- *Normal conduction velocity* corresponds to a scenario wherein the gap junction is working properly. The conduction velocity in this case is 50 cm/s. This scenario corresponds to $N_{\text{channel}} = 6700$.
- *Half conduction velocity* corresponds to a scenario wherein a 50% reduction in the conduction velocity occurs due to damages in the cardiac tissue. The conduction velocity in this case is 25.6 cm/s and it corresponds to $N_{\text{channel}} = 1850$.
- *Block-threshold velocity* corresponds to a scenario wherein the conduction velocity is at its lowest possible level where nondecremental propagation can still be sustained. The conduction velocity in this case is 0.91 cm/s and it corresponds to $N_{\text{channel}} = 85$.

B. THE MEMBRANE POTENTIAL EFFECT

According to [10] and [28], the hemichannels also show a minor sensitivity, called V_m-gating, to the membrane potentials V_{m1} and V_{m2}, in addition to their main dependency on V_j. This sensitivity does not affect the properties of the V_j-gating process and applies its effect when a hemichannel is in its *high* conductance state [28]. We expressed the V_m-gating effect for a hemichannel with total conductance g_t in [10] as

$$\begin{cases} g_t = g_H - C(V_j)V_m & \text{for } \textit{high} \text{ state}\\ g_t = g_L & \text{for } \textit{low} \text{ state,}\end{cases} \quad (13)$$

where g_L is the conductance in the *low* state, g_H is the conductance in the *high* state, and $C(V_j)$ is a linearly decreasing function of V_j. This function governs the effect of the membrane potential on the hemichannel conductance.

Due to the steepness and absolute value of V_m-gating function being considerably smaller in comparison to those of V_j-gating [28], $C(V_j)V_m$ can be reasonably approximated with its mean value. By denoting the average of $C(V_j)V_m$ over V_m as $\overline{g_m}$, Eq. (13) can be written as

$$\begin{cases} g_t \approx g_H - \overline{g_m} & \text{for } \textit{high} \text{ state}\\ g_t = g_L & \text{for } \textit{low} \text{ state.}\end{cases} \quad (14)$$

We use this approximation throughout the paper. The numerical value of $\overline{g_m}$ is provided in Appendix.

C. RESISTANCE STATES OF A SINGLE BRANCH

We compute the resistances of the four gap junction states based on the presented model, and then use in the following section to derive the noise expressions for the states.

In the HH state, the conductances of the hemichannels Cx1 and Cx2 can be written as

$$\begin{aligned} g_{1_{HH}} &= \lambda_{H_1} e^{\frac{V_j}{V_{0_{H_1}}}\frac{g_{2_{HH}}}{g_{1_{HH}}+g_{2_{HH}}}} - \overline{g_{m_1}},\\ g_{2_{HH}} &= \lambda_{H_2} e^{\frac{V_j}{V_{0_{H_2}}}\frac{g_{1_{HH}}}{g_{1_{HH}}+g_{2_{HH}}}} - \overline{g_{m_2}}. \end{aligned} \quad (15)$$

Assuming that the current flow through the junction is I_j, the total resistance of the channel can be written as

$$R_{HH} = \frac{V_j}{I_j} = \frac{1}{g_{1_{HH}}} + \frac{1}{g_{2_{HH}}}. \quad (16)$$

Similarly, the conductances of the hemichannels in the HL, LH and LL states can be written respectively as

$$\begin{aligned} g_{1_{HL}} &= \lambda_{H_1} e^{\frac{V_j}{V_{0_{H_1}}}\frac{g_{2_{HL}}}{g_{1_{HL}}+g_{2_{HL}}}} - \overline{g_{m_1}},\\ g_{2_{HL}} &= \lambda_{L_2} e^{\frac{V_j}{V_{0_{L_2}}}\frac{g_{1_{HL}}}{g_{1_{HL}}+g_{2_{HL}}}}, \end{aligned} \quad (17)$$

$$\begin{aligned} g_{1_{LH}} &= \lambda_{L_1} e^{\frac{V_j}{V_{0_{L_1}}}\frac{g_{2_{LH}}}{g_{1_{LH}}+g_{2_{LH}}}},\\ g_{2_{LH}} &= \lambda_{H_2} e^{\frac{V_j}{V_{0_{H_2}}}\frac{g_{1_{LH}}}{g_{1_{LH}}+g_{2_{LH}}}} - \overline{g_{m_2}}, \end{aligned} \quad (18)$$

$$\begin{aligned} g_{1_{LL}} &= \lambda_{L_1} e^{\frac{V_j}{V_{0_{L_1}}}\frac{g_{2_{LL}}}{g_{1_{LL}}+g_{2_{LL}}}},\\ g_{2_{LL}} &= \lambda_{L_2} e^{\frac{V_j}{V_{0_{L_2}}}\frac{g_{1_{LL}}}{g_{1_{LL}}+g_{2_{LL}}}}, \end{aligned} \quad (19)$$

and the total resistance of the branch can be written as

$$R_i = \begin{cases} \frac{1}{g1_{HH}} + \frac{1}{g2_{HH}} & i = HH \\ \frac{1}{g1_{HL}} + \frac{1}{g2_{HL}} & i = HL \\ \frac{1}{g1_{LH}} + \frac{1}{g2_{LH}} & i = LH \\ \frac{1}{g1_{LL}} + \frac{1}{g2_{LL}} & i = LL. \end{cases} \tag{20}$$

III. CAPACITY DERIVATION

In this section, we first find expressions for noise for the four states of the state-machine presented in the previous section. Subsequently, we derive expressions for capacities of the individual channel states. Ultimately, we present an information theoretical analysis to derive the total capacity of the channel.

From an information theoretical point of view, the state-machine presented in Section II-A acts as a communication channel which has different states, with each state corresponding to specific channel quality. In the information theory literature, this type of channel is known as a Finite-State Channel (FSC) [30]. If, however, the transition between the states is governed by a Markov process, the channel is referred to as a Finite-State Markov channel (FSMC) [31]. By partitioning the range of the received signal-to-noise ratio (SNR) into a finite number of intervals, FSMCs can, for example, be constructed for Rayleigh fading channels [31].

According to [30], a finite-state channel is a channel with the state sequence $\mathbf{s} = \{\ldots, s_{-1}, s_0, s_1, \ldots\}$. Assuming the input and output sequences to be $\{\ldots, x_{-1}, x_0, x_1, \ldots\}$ and $\{\ldots, y_{-1}, y_0, y_1, \ldots\}$, respectively, the channel can be described statistically by a conditional probability assignment $P(y_n s_n | x_n s_{n-1})$. This assignment is independent of n and denotes the following:

- For a given time n, all of the relevant past is summarized into a state variable s_{n-1}.
- The output from the channel, y_n, and the new state, s_n, can be defined by a probability measure on $\{y_n, s_n\}$ conditioned on $\{x_n, s_{n-1}\}$.

So far, FSCs have been mainly used to model (a) flat-fading channels, wherein the channel state is a random variable which is independent of channel inputs, and (b) intersymbol-interference channels, wherein the channel state is a deterministic function of the channel inputs.

In our scenario, however, the channel state is a discrete random variable which is correlated to the channel inputs. To elaborate, the channel has four states which are governed by a first-order Markov chain. We will show in the next subsection that each of these states corresponds to a different noise level and the channel probability can be described by the FSC form.

A. NOISE EXPRESSIONS

According to [32], the random motion of charge carriers in a conducting or semiconducting medium generates a noise power of

$$N = 4k_B TR, \tag{21}$$

where k_B is Boltzmann's constant, T is the temperature in Kelvin and R is the resistance of the medium. This phenomenon is called the Johnson-Nyquist noise and applies to charge carriers in any type of conducting medium (e.g., ions in the electrolyte), not just resistors. The Johnson-Nyquist noise has a power spectrum that is flat to more than 10^{12} Hz which is much larger than that of most systems of interest, including gap junction channels. This implies that the power spectral density of this noise can be assumed to be constant. One can also assume that the Johnson-Nyquist noise has a Gaussian amplitude probability density function. The reason is that this noise is caused by the random motion of charge carriers, with each charge carrier having a small contribution to the total noise. Hence, the Gaussian assumption can be justified through the central-limit theorem [32]. We use the additive white Gaussian noise model throughout the paper.

From Eqs. (20) and (21), the noise powers of the states $i \in \{HH, HL, LH, LL\}$ can be written as

$$N_i = \begin{cases} 4k_B TR_{HH} & i = HH \\ 4k_B TR_{HL} & i = HL \\ 4k_B TR_{LH} & i = LH \\ 4k_B TR_{LL} & i = LL. \end{cases} \tag{22}$$

B. CAPACITIES OF INDIVIDUAL CHANNEL STATES

The individual channel states can accordingly be seen as Additive white Gaussian noise (AWGN) channels with different levels of noise. Their information capacities can be computed from the AWGN channel capacity formula:

$$C = \frac{1}{2}\log_2\left(1 + \frac{P}{N}\right), \tag{23}$$

where P is the signal power constraint and N is the noise power [33]. From Eqs. (22) and (23), the capacities of the four mentioned states of the channel can be written as

$$C_i = \begin{cases} \frac{1}{2}\log_2\left(1 + \frac{P}{N_{HH}}\right) & i = HH \\ \frac{1}{2}\log_2\left(1 + \frac{P}{N_{HL}}\right) & i = HL \\ \frac{1}{2}\log_2\left(1 + \frac{P}{N_{LH}}\right) & i = LH \\ \frac{1}{2}\log_2\left(1 + \frac{P}{N_{LL}}\right) & i = LL. \end{cases} \tag{24}$$

C. TOTAL CAPACITY FORMULATION

In the following theorem, we derive a closed-form expression for the capacity of the total gap junction channel.

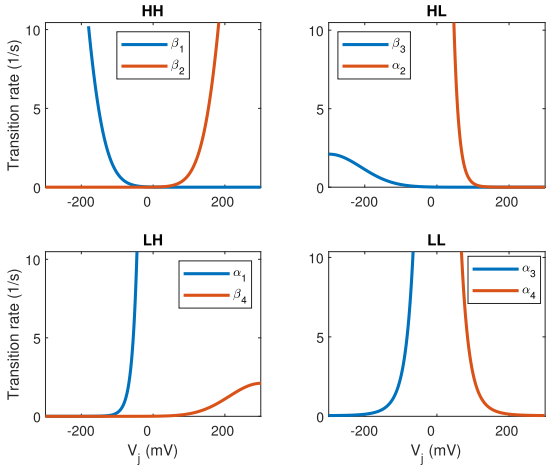

FIGURE 4. Transition rates in Eq. (10) between the four states of the Markov chain as functions of V_j.

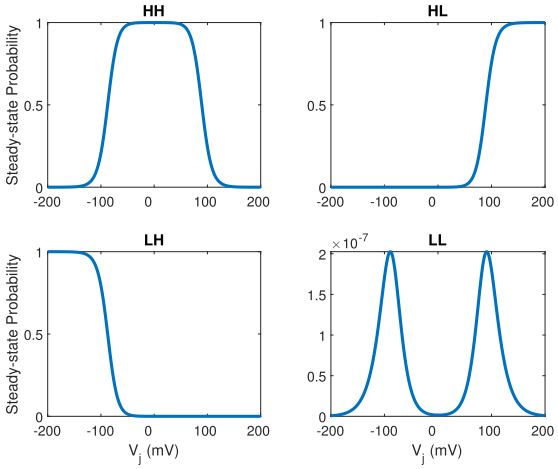

FIGURE 5. Steady-state probabilities of the four channel states as functions of V_j.

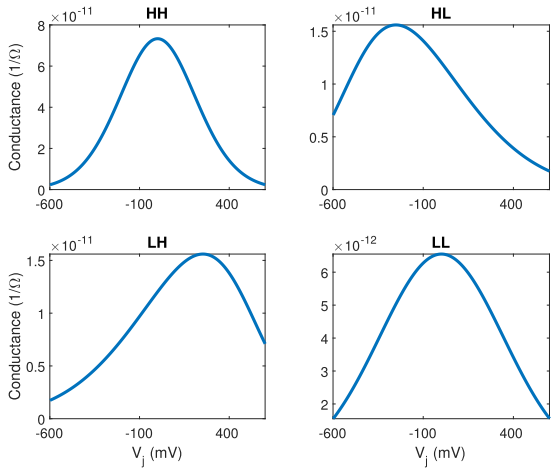

FIGURE 6. Conductances of a the single gap junction channel in the four states as functions of V_j.

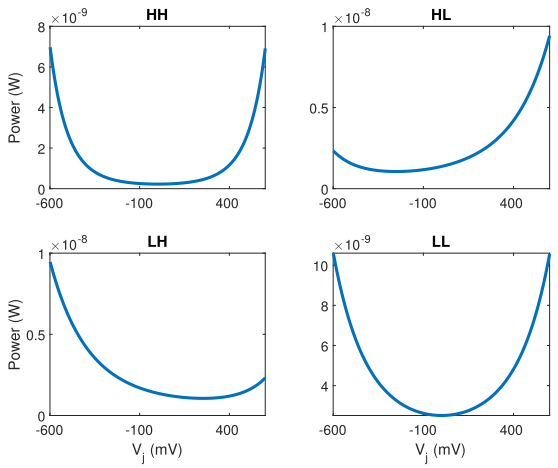

FIGURE 7. Noise powers generated in each of the four channel states as functions of V_j.

Theorem 1: The capacity of the gap junction channel shown in Fig. 3 can be written as

$$C = \sum_{i=1}^{4} \pi_i C_i, \tag{25}$$

where π_i is the steady-state distribution of gap junction states and C_i is the single branch capacity from Eq. (24).

Proof 1: The mutual information between the random input and the random output process is

$$I(X;Y) = H(Y) - H(Y|X) \tag{26}$$

where $H(Y)$ and $H(Y|X)$ are the entropy rate of the output process and the entropy rate of the output process given the input process, respectively. According to the system model, it can be seen that when the gap junction is in state i, the mutual information is

$$I(X;Y|i) = \frac{1}{2}\log_2\left(1 + \frac{P}{N_i}\right) \tag{27}$$

where N_i is the noise power of state i [34]. Since π_i determines the long-run proportion of the channel states, one can write

$$\begin{aligned} I(X;Y) &= \sum_{i=1}^{4} \pi_i I(X;Y|i) \\ &= \sum_{i=1}^{4} \pi_i C_i. \end{aligned} \tag{28}$$

An analogous capacity derivation for an FSMC based on its steady-state probabilities can be found in [35, Sec. 4.7.1].

IV. NUMERICAL RESULTS

We present a numerical representation of the achievable rates derived in the previous section using the framework implemented in MATLAB. We use the parameters given in [29] for the most abundant hemichannel combination in the heart, Cx43-Cx43, which is made of two identical Cx43 proteins, to feed Eqs. (6) and (10). Afterwards, we present numerical evaluations for the single-state and total capacities.

Fig. 4 shows the transition rates for each of the four states for different V_js. Although these rates are functions of (V_{j1}, V_{j2}) and not directly of V_j, they still show exponential behaviors. The reason for this is that the relation between V_j and (V_{j1}, V_{j2}) is almost linear. Referring to the figures that

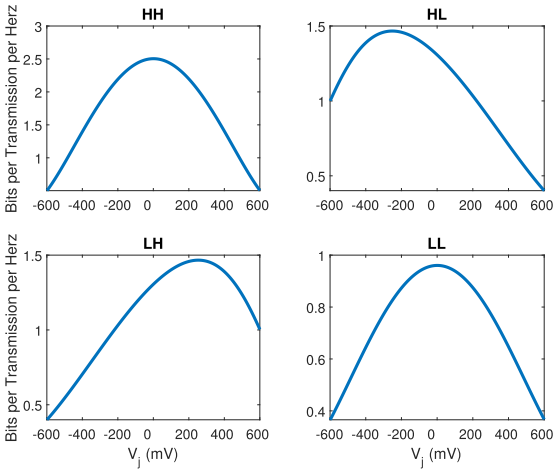

FIGURE 8. Capacities of the individual states for fixed signal power $P = 7 \times 10^{-9}$ as functions of V_j.

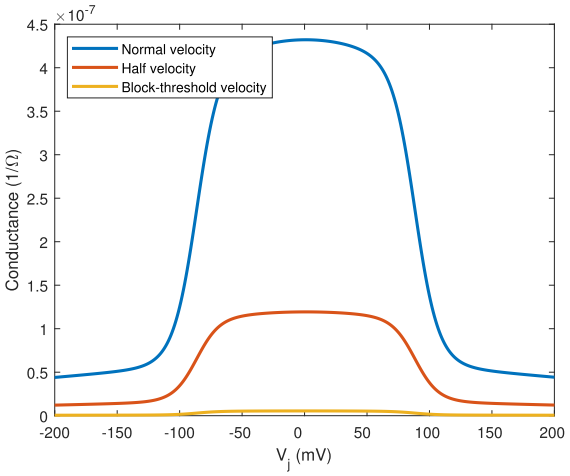

FIGURE 9. The total steady-state conductances of a gap junction channel in three different modes; Normal conduction velocity 50 cm/s, half conduction velocity 25.6 cm/s, and block-threshold conduction velocity 0.91 cm/s states, as functions of V_j.

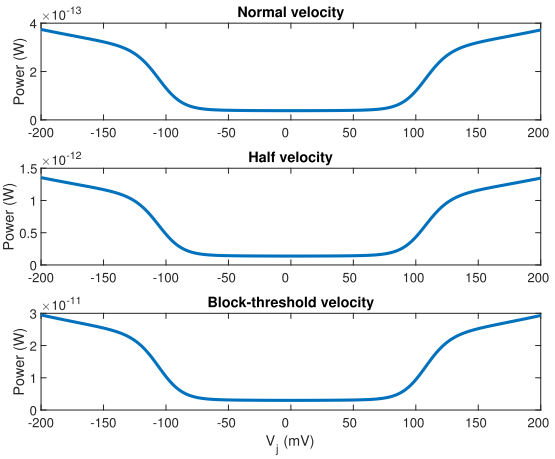

FIGURE 10. The total noise powers generated in the gap junction in the three conduction velocity states as functions of V_j.

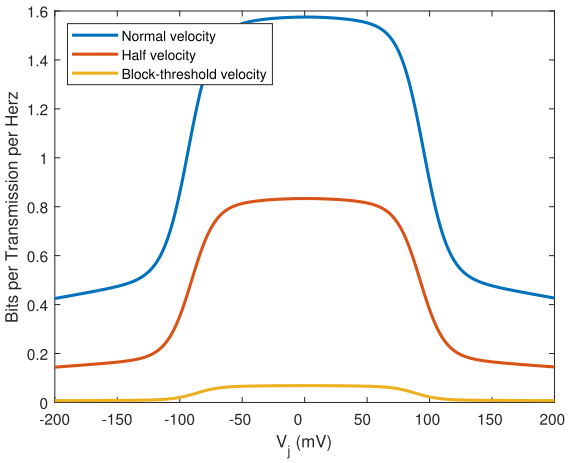

FIGURE 11. Comparison of the total capacities of the gap junction channel for the three conduction velocities as functions of V_j.

show the output rates for the HH and HL states, we observe that β_1 in the figure for the HH state is considerably different from β_3 in the figure for the LL state. As seen from Eq. 10, both β_1 and β_3 are functions of V_{j1} and the parameters of these functions are identical. The reason for the curves of β_1 and β_3 to be different from each other is that V_{j1} in state HH is different from V_{j1} in state HL. This leads to two different voltage distributions along the hemichannels. The same applies to β_4 and β_2.

Fig. 5 shows the steady state probabilities of the four states of the Markov chain shown in Fig. 3. It can be seen that the LH, HH, and HL states dominate in the low, middle, and high transjunctional voltage ranges, respectively. Although the probabilities of the LL state are very low and close to zero, the state is still taken into account in our analysis.

Fig. 6 shows the conductances for the four channel states. It can be seen that the curves for the HH and LL states are symmetric, whereas the curves for the HL and LH states have their maximums in negative and positive V_js, respectively. They also show that the conductance in the HH state is almost one order of magnitude larger than that of the LL state.

Fig. 7 shows the generated noise powers in all channel states. The curves are based on Eq. (22). It can be seen that, for a single gap junction channel, the values of the noise in the four states do not differ significantly from each other.

Fig. 8 shows the capacities of individual gap junction states for a fixed signal power $P = 7 \times 10^{-9}$ W. This signal power is chosen based on the noise powers in Fig. 7. It can be seen that the capacity curves of the HH and LL states are symmetrical, while the ones for LH and HL states are asymmetrical. The reason for this is that the peak of the capacity curves corresponds to the voltages where the total conductances reach their maximum. The maximum occurs at non-zero voltages when the conductance states of the hemichannels are different from each other.

Fig. 9 shows the total conductance of a gap junction channel in the steady-state for three different conduction modes. These curves are produced by calculating the weighted sum of the conductances in Fig. 6 according to their steady-state probabilities in Fig. 5, and multiplying the results by the number of channels corresponding to each conduction state of

the gap junction, as stated in Section II-A. The conductance offsets are also applied. The blue curve corresponds to a gap junction in its normal conducting state. The red and the yellow curves correspond to half velocity and block-threshold velocity states, respectively. It can be seen that a 50 % reduction in velocity corresponds to a greater reduction in the conductance, as the conductances in the half velocity curve are less than half of their equivalents in the normal velocity curve.

Fig. 10 shows the total steady-state noise powers generated in the gap junction in the three conduction velocity states. The curves are produced from Eq. (21) with the conductance values shown in Fig. 9. The differences between the noise powers follow the same proportions as between the conductances.

Ultimately, Fig. 11 shows the total information capacity of the gap junction channel for the three conduction velocity states as a function of V_j. It can be seen that the capacity curves approximately follow the proportions of the conduction velocities, e.g., the values of the half velocity curve are almost half of their equivalents in the normal velocity curve. The differences between the capacity curves are not as large as the ones between the conductance curves in Fig. 8. This is mainly due to the logarithmic nature of the capacity function.

V. CONCLUSION

In this paper, we used a mathematical model for a single-branch gap junction channel as the basis of the information theoretical analysis. In the model, the gap junction branch is a serial combination of two hemichannels, with each hemichannel having the two conductance states *high* and *low*. The whole gap junction is then formulated as a four-state Markov chain. First, we found expressions for noise for each of the four states in the model. Secondly, the capacities of the individual states were computed using the Gaussian channel model. Thirdly, we used the finite-state channel model to analytically derive the total capacity of the gap junction. Finally, numerical representations of the results were given.

The results obtained in the analysis of cardiac gap junctions show that the capacity of a gap junction channel is at its maximum in the approximate transjunctional voltage range of $[-75, 75]$ mV. The capacity drops by around 70 % in the voltage ranges lower than -100 and higher than 100 mV. They also show that reductions of the conduction velocity in the gap junction lead to proportional reductions in the capacity. For instance, the capacity of a gap junction in half conduction velocity scenario is nearly half of the capacity in the normal conduction velocity scenario.

APPENDIX A
NUMERICAL VALUES OF PARAMETERS

In this part, the numerical values for the constants and parameters throughout the paper are given.

The parameters in Eqs. (8) and (9) for Cx43 hemichannels are given in [29] as follows:

$$\lambda_{H1} = \lambda_{H2} = 146.6 \text{ pS},$$
$$\lambda_{L1} = \lambda_{L2} = 13.1 \text{ pS},$$
$$V_{0_{H1}} = V_{0_{H2}} = 145.9 \text{ mV},$$
$$V_{0_{L1}} = V_{0_{L2}} = 299 \text{ mV}.$$

The rate coefficients in Eq. (10) are presented in [29] as follows:

$$\alpha_1 = \alpha_3 = \frac{2\alpha_{\text{coef}}}{1 + \exp(-Vj_1/V_\alpha)},$$
$$\alpha_2 = \alpha_4 = \frac{2\alpha_{\text{coef}}}{1 + \exp(-Vj_2/V_\alpha)},$$
$$\beta_1 = \beta_3 = \beta_{\text{coef}} \exp(-Vj_1/V_\beta),$$
$$\beta_2 = \beta_4 = \beta_{\text{coef}} \exp(-Vj_2/V_\beta),$$

where

$$\alpha_{\text{coef}} = 181.5 \text{ s}^{-1},$$
$$\beta_{\text{coef}} = 0.007 \text{ s}^{-1},$$
$$V_\alpha = 8.347 \text{ mV},$$
$$V_\beta = 8.675 \text{ mV}.$$

The conductance offset in Eq. (14) is calculated from the data available in [28] and follows as:

$$\overline{g_m} = 5.8 \times 10^{-8} \text{ S},$$

for the non-normalized conductance and

$$\overline{g_m} = 0.12\text{G}_{\text{jss}},$$

for the normalized conductance (G_{jss}, as described in [28]).

REFERENCES

[1] R. M. Shubair and H. Elayan, "*In vivo* wireless body communications: State-of-the-art and future directions," in *Proc. Loughborough Antennas Propag. Conf. (LAPC)*, Nov. 2015, pp. 1–5.

[2] I. F. Akyildiz, J. M. Jornet, and M. Pierobon, "Nanonetworks: A new frontier in communications," *Commun. ACM*, vol. 54, no. 11, pp. 84–89, Nov. 2011.

[3] L. Felicetti, M. Femminella, G. Reali, and P. Liò, "Applications of molecular communications to medicine: A survey," *Nano Commun. Netw.*, vol. 7, pp. 27–45, Mar. 2016.

[4] T. Nakano, M. Moore, A. Enomoto, and T. Suda, "Molecular communication technology as a biological ICT," in *Biological Functions for Information and Communication Technologies*. Berlin, Germany: Springer, 2011, pp. 49–86.

[5] B. Atakan, O. Akan, and S. Balasubramaniam, "Body area nanonetworks with molecular communications in nanomedicine," *IEEE Commun. Mag.*, vol. 50, no. 1, pp. 28–34, Jan. 2012.

[6] I. Akyildiz, M. Pierobon, S. Balasubramaniam, and Y. Koucheryavy, "The Internet of bio-nano things," *IEEE Commun. Mag.*, vol. 53, no. 3, pp. 32–40, Mar. 2015.

[7] N. Farsad, "Molecular communication: Interconnecting tiny nanobio devices," *GetMobile, Mobile Comput. Commun.*, vol. 22, no. 2, pp. 5–10, Sep. 2018.

[8] J. M. Jornet and I. F. Akyildiz, "Channel modeling and capacity analysis for electromagnetic wireless nanonetworks in the terahertz band," *IEEE Trans. Wireless Commun.*, vol. 10, no. 10, pp. 3211–3221, Oct. 2011.

[9] V. Jamali, A. Ahmadzadeh, C. Jardin, C. Sticht, and R. Schober, "Channel estimation for diffusive molecular communications," *IEEE Trans. Commun.*, vol. 64, no. 10, pp. 4238–4252, Oct. 2016.

[10] F. Hejri, M. Veletić, and I. Balasingham, "On the cardiac gap junctions channel modeling," in *Proc. 6th Annu. ACM Int. Conf. Nanosc. Comput. Commun.*, Sep. 2019, pp. 1–6.

[11] M. Kuscu, E. Dinc, B. A. Bilgin, H. Ramezani, and O. B. Akan, "Transmitter and receiver architectures for molecular communications: A survey on physical design with modulation, coding, and detection techniques," *Proc. IEEE*, vol. 107, no. 7, pp. 1302–1341, Jul. 2019.

[12] T. Nakano, Y. Okaie, S. Kobayashi, T. Hara, Y. Hiraoka, and T. Haraguchi, "Methods and applications of mobile molecular communication," *Proc. IEEE*, vol. 107, no. 7, pp. 1442–1456, Jul. 2019.
[13] Y. M. Gao, S. H. Pun, P. U. Mak, M. Du, and M. I. Vai, "Preliminary modeling for intra-body communication," in *Proc. 13th Int. Conf. Biomed. Eng.*, C. T. Lim and J. C. H. Goh, Eds. Berlin, Germany: Springer, 2009, pp. 1044–1048.
[14] M. Veletić and I. Balasingham, "An information theory of neurotransmission in multiple-access synaptic channels," *IEEE Trans. Commun.*, vol. 68, no. 2, pp. 841–853, Feb. 2020.
[15] C. Rose and I. S. Mian, "Inscribed matter communication: Part I," *IEEE Trans. Mol., Biol. Multi-Scale Commun.*, vol. 2, no. 2, pp. 209–227, Dec. 2016.
[16] C. Rose and I. S. Mian, "Inscribed matter communication: Part II," *IEEE Trans. Mol., Biol. Multi-Scale Commun.*, vol. 2, no. 2, pp. 228–239, Dec. 2016.
[17] P. Mueller and D. O. Rudin, "Induced excitability in reconstituted cell membrane structure," *J. Theor. Biol.*, vol. 4, no. 3, pp. 268–280, May 1963.
[18] G. Ehrenstein, H. Lecar, and R. Nossal, "The nature of the negative resistance in bimolecular lipid membranes containing excitability-inducing material," *J. Gen. Physiol.*, vol. 55, no. 1, pp. 119–133, Jan. 1970.
[19] D. C. Spray, A. L. Harris, and M. V. Bennett, "Equilibrium properties of a voltage-dependent junctional conductance," *J. Gen. Physiol.*, vol. 77, no. 1, pp. 77–93, Jan. 1981.
[20] R. Vogel and R. Weingart, "Mathematical model of vertebrate gap junctions derived from electrical measurements on homotypic and heterotypic channels," *J. Physiol.*, vol. 510, no. 1, pp. 177–189, Jul. 1998.
[21] A. Revilla, C. Castro, and L. C. Barrio, "Molecular dissection of transjunctional voltage dependence in the connexin-32 and connexin-43 junctions," *Biophys. J.*, vol. 77, no. 3, pp. 1374–1383, Sep. 1999.
[22] S. Baigent, J. Stark, and A. Warner, "Modelling the effect of gap junction nonlinearities in systems of coupled cells," *J. Theor. Biol.*, vol. 186, no. 2, pp. 223–239, May 1997.
[23] S. Baigent, J. Stark, and A. Warner, "Convergent dynamics of two cells coupled by a nonlinear gap junction," *Nonlinear Anal., Theory, Methods Appl.*, vol. 47, no. 1, pp. 257–268, Aug. 2001.
[24] S. Baigent, "Cells coupled by voltage-dependent gap junctions: The asymptotic dynamical limit," *Biosystems*, vol. 68, nos. 2–3, pp. 213–222, Feb. 2003.
[25] P. Donnell, S. A. Baigent, and M. Banaji, "Monotone dynamics of two cells dynamically coupled by a voltage-dependent gap junction," *J. Theor. Biol.*, vol. 261, no. 1, pp. 120–125, Nov. 2009.
[26] T. Nakano, T. Suda, T. Koujin, T. Haraguchi, and Y. Hiraoka, "Molecular communication through gap junction channels: System design, experiments and modeling," in *Proc. 2nd Bio-Inspired Models Netw., Inf. Comput. Syst.*, Dec. 2007, pp. 139–146.
[27] D. Kilinc and O. B. Akan, "An information theoretical analysis of nanoscale molecular gap junction communication channel between cardiomyocytes," *IEEE Trans. Nanotechnol.*, vol. 12, no. 2, pp. 129–136, Mar. 2013.
[28] L. C. Barrio, A. Revilla, J. M. Goméz-Hernandez, M. de Miguel, and D. González, "Membrane potential dependence of gap junctions in vertebrates," in *Current Topics in Membranes*, vol. 49, C. Peracchia, Ed. New York, NY, USA: Academic, 1999, ch. 8, pp. 175–188.
[29] A. P. Henriquez, R. Vogel, B. J. Muller-Borer, C. S. Henriquez, R. Weingart, and W. E. Cascio, "Influence of dynamic gap junction resistance on impulse propagation in ventricular myocardium: A computer simulation study," *Biophys. J.*, vol. 81, no. 4, pp. 2112–2121, Oct. 2001.
[30] R. G. Gallager, *Information Theory and Reliable Communication*, vol. 2. New York, NY, USA: Wiley, 1968.
[31] H. S. Wang and N. Moayeri, "Finite-state Markov channel—A useful model for radio communication channels," *IEEE Trans. Veh. Technol.*, vol. 44, no. 1, pp. 163–171, Feb. 1995.
[32] W. H. Tranter and R. E. Ziemer, *Principles of Communications: Systems, Modulation, and Noise*. Hoboken, NJ, USA: Wiley, 1995.
[33] T. M. Cover and J. A. Thomas, *Elements of Information Theory*. Hoboken, NJ, USA: Wiley, 2012.
[34] A. J. Goldsmith and P. P. Varaiya, "Capacity, mutual information, and coding for finite-state Markov channels," *IEEE Trans. Inf. Theory*, vol. 42, no. 3, pp. 868–886, May 1996.
[35] H. D. Pfister, "On the capacity of finite state channels and the analysis of convolutional accumulate-m codes," Ph.D. dissertation, Dept. Elect. Comput. Eng., Univ. California, San Diego, La Jolla, CA, USA, 2003.

FARROKH HEJRI received the bachelor's degree in electrical engineering from the Hamedan University of Technology, Iran, in 2012, and the master's degree in communication systems from the Amirkabir University of Technology, Tehran, Iran. He is currently pursuing the Ph.D. degree with the Department of Electronic Systems, Norwegian University of Science and Technology (NTNU), where he works mainly on communication-theoretic modeling of the heart. His research interests include information theory, communication theory, and stochastic processes.

MLADEN VELETIĆ received the B.Sc. and M.Sc. degrees in electronics and telecommunications from the Faculty of Electrical Engineering, University of Banja Luka (UNIBL), Bosnia and Herzegovina, in 2010 and 2012, respectively, and the joint Ph.D. degree in telecommunications from the Department of Electronic Systems, Norwegian University of Science and Technology (NTNU), Norway, and the Faculty of Electrical Engineering, UNIBL. From 2011 to 2017, he worked as a Senior Teaching and a Research Assistant with the University of Banja Luka. He is currently a Postdoctoral Research Scientist with The Intervention Center, Oslo University Hospital. His research interests include molecular and nano-neural communications, wireless communications, and positioning in cellular networks. He was awarded the Gold Plaque from the UNIBL for his achievements throughout the undergraduate education.

ILANGKO BALASINGHAM (Senior Member, IEEE) received the M.Sc. and Ph.D. degrees in signal processing from the Department of Electronics and Telecommunications, Norwegian University of Science and Technology (NTNU), Trondheim, Norway, in 1993 and 1998, respectively. He performed his master's degree thesis at the Department of Electrical and Computer Engineering, University of California at Santa Barbara, Santa Barbara, CA, USA. From 1998 to 2002, he was a Research Engineer developing image and video streaming solutions for mobile handheld devices with Fast Search & Transfer ASA, Oslo, Norway, which is currently a part of Microsoft Inc. Since 2002, he has been a Senior Research Scientist with The Intervention Center, Oslo University Hospital, Oslo, where he heads the Wireless Sensor Network Research Group. He was appointed as a Professor in signal processing in medical applications with NTNU, in 2006. From 2016 to 2017, he was a Professor (by courtesy) with the Frontier Institute, Nagoya Institute of Technology, Japan. He has authored or coauthored more than 200 journals and conference papers, seven book chapters, 42 abstracts, and 16 articles in popular press, and holds five patents. His research interests include super robust short range communications for both inbody and onbody sensors, body area sensor networks, microwave short range sensing of vital signs, short range localization and tracking mobile sensors, and nanoscale communication networks. He has given 16 invited/keynotes at the international conferences. In addition, he is active in organizing conferences (has also been a Steering Committee Member of ACM NANOCOM, since 2018, the General Chair of the 2019 IEEE International Symposium of Medical ICT and the 2012 Body Area Networks Conference, and the TPC Chair of the 2015 ACM NANOCOM), and an Editorial Board (has been an Area Editor of *Nano Communication Networks* (Elsevier), since 2013).